

# Concerted Interconversion between Ionic Lock Substates of the $\beta_2$ Adrenergic Receptor Revealed by Microsecond Timescale Molecular Dynamics

Tod D. Romo,<sup>†</sup> Alan Grossfield,<sup>†\*</sup> and Michael C. Pitman<sup>‡</sup>

<sup>†</sup>Department of Biochemistry and Biophysics, University of Rochester Medical School, Rochester, New York; and <sup>‡</sup>IBM, T. J. Watson Research Center, Yorktown Heights, New York

**ABSTRACT** The recently solved crystallographic structures for the A<sub>2A</sub> adenosine receptor and the  $\beta_1$  and  $\beta_2$  adrenergic receptors have shown important differences between members of the class-A G-protein-coupled receptors and their archetypal model, rhodopsin, such as the apparent breaking of the ionic lock that stabilizes the inactive structure. Here, we characterize a 1.02  $\mu$ s all-atom simulation of an apo- $\beta_2$  adrenergic receptor that is missing the third intracellular loop to better understand the inactive structure. Although we find that the structure is remarkably rigid, there is a rapid influx of water into the core of the protein, as well as a slight expansion of the molecule relative to the crystal structure. In contrast to the x-ray crystal structures, the ionic lock rapidly reforms, although we see an activation-precursor-like event wherein the ionic lock opens for ~200 ns, accompanied by movements in the transmembrane helices associated with activation. When the lock reforms, we see the structure return to its inactive conformation. We also find that the ionic lock exists in three states: closed (or locked), semi-open with a bridging water molecule, and open. The interconversion of these states involves the concerted motion of the entire protein. We characterize these states and the concerted motion underlying their interconversion. These findings may help elucidate the connection between key local events and the associated global structural changes during activation.

## INTRODUCTION

The G-protein-coupled receptor (GPCR) family of membrane proteins comprises the largest group of membrane proteins in the human genome. These proteins are the targets of many drugs, and GPCR mutations are responsible for many diseases (1–3). One study found more than 5000 unique GPCR sequences among 13 different species, including 865 from humans (4). These proteins share a similar structural motif consisting of a heptahelical transmembrane (TM) core with an eighth helix oriented in the plane of the membrane. Historically, the structural archetype for GPCRs has been rhodopsin, because it is readily available from bovine retinas and has sufficient structural stability to permit its crystallization. Unlike rhodopsin, however, most GPCRs function more like rheostats than like switches, and exist in a spectrum of conformational substates (2,5).

Recently solved crystallographic structures of  $\beta_2$ -adrenergic receptor (B2AR) have shown important differences between B2AR and rhodopsin, including an apparent disruption of the “ionic lock”. The ionic lock is a common feature of many GPCRs and is part of the conserved (D/E)RY motif at the intracellular (IC) end of TM3. This motif forms an intrahelical salt bridge between the D130 and R131 (in B2AR), as well as an interhelical salt bridge between TM3 and TM6 (R131 and E268 in B2AR) that stabilizes the inactivated form of B2AR (6–11). Disruption of this lock has been shown to be a required step for activation, and it occurs

upon binding of nearly all agonists (2,9). In addition, mutations of the lock residues lead to constitutively active mutants (9). For this reason, it is surprising that the crystallographic models of GPCRs (other than rhodopsin) show the lock as broken (6,7,12–14). This has led to speculation that the lock may not be a universal mechanism in GPCRs (13,15).

In this work, we address some of these questions by analyzing a 1.02  $\mu$ s all-atom molecular-dynamics (MD) simulation of B2AR-T4 fusion protein solved by Cherezov et al. (6), with the lysozyme and carazolol ligand removed. We find that the ionic lock reforms and is “noisy”, and that the B2AR structure is remarkably rigid. Despite this, we see concerted motions suggestive of activation-precursor events. We also find that the core of the protein rapidly hydrates and stays hydrated throughout the simulation.

## MATERIALS AND METHODS

The starting structure for our simulations was the x-ray crystallographic structure of the carazolol-bound B2AR/T4-lysozyme fusion protein (2RH1) solved by Cherezov et al. (6). The T4-lysozyme was removed, leaving the attachment points with the ICL3 unattached, with the clipped termini unbonded. It was previously shown experimentally that partial removal of ICL3 results in functional protein (16); therefore, removal of the T4 during system construction for the MD simulation was not expected to significantly alter the protein’s potential functional properties and hence expected fluctuations. In addition, the carazolol ligand was removed to increase the likelihood that fluctuations resembling activation-like processes (i.e., fluctuations that resemble the precursors to activation) would occur on the MD timescale.

The protein was embedded in a lipid bilayer consisting of 99 1-palmitoyl-2-oleoyl-phosphatidylcholine lipids, and the entire system was solvated with

Submitted July 17, 2009, and accepted for publication September 21, 2009.

\*Correspondence: alan\_grossfield@urmc.rochester.edu

Editor: Nathan Andrew Baker.

© 2010 by the Biophysical Society  
0006-3495/10/01/0076/9 \$2.00

doi: 10.1016/j.bpj.2009.09.046

7000 explicit water molecules, including the intraprotein crystallographic waters. The protonation state of titratable residues was set to be consistent with a physiological pH (i.e., all glutamate and aspartate residues were deprotonated). We added 13 Na<sup>+</sup> and 15 Cl<sup>-</sup> ions, to obtain a net neutral system with ~100 mM salt, resulting in a total simulation size of 38,938 atoms. The CHARMM22 (17,18) force field was used to represent the protein along with the most recent CHARMM27 lipid and cholesterol parameters (19,20), in addition to P3M Ewald (21,22) for electrostatics and a 10 Å van der Waals cutoff. The temperature was held at 310 K by means of an Andersen thermostat with a 1 ns resample time, and a 2 fs step size was used with bonds constrained to their equilibrium lengths using RATTLE (23). The system was equilibrated using a 29 ns simulation in the NPAT (constant number of molecules, normal pressure, area, and temperature) ensemble using NAMD (24). Then, a total of 1.02 μs were simulated in the NVT ensemble using Blue Matter (25) on the Blue Gene/W supercomputer located at IBM Watson (26). The NVT ensemble was used rather than NPAT because the latter is not supported by Blue Matter, and since the simulation was run with a high node count, the performance difference between NAMD (24) and Blue Matter is significant. In addition, data from previously published simulations of dark and activated light rhodopsin, obtained using similar MD protocols (in the NVE ensemble) and an analogous assembly, were used for comparison (27,28).

Unless otherwise noted, all analyses were performed using a trajectory subsampled at 1 ns resolution. The data were analyzed using the Lightweight Object-Oriented Structure (LOOS) analysis library and toolset developed in our laboratory. LOOS is an open-source library that uses C++ and BOOST, and provides a framework for rapidly and easily creating new analytical tools (<http://loos.sourceforge.net>) (29). Implementation details regarding analyses using LOOS can be found in the Supporting Material.

## RESULTS AND DISCUSSION

### Global motions

The average root mean-square displacement (RMSD) between the simulation and the crystal structure, computed over TM α-carbons only, is 1.7 Å. Most of the drift from the starting crystal structure occurs during the first few nanoseconds of the 29 ns equilibration run, after which the protein is very rigid. Most of the fluctuations in the B2AR structure occur at the ends of the TM helices and in the IC and extracellular (EC) loops. Although the loop fragments at the end of TM5 and TM6 (where the clipped ICL3 was removed) are quite flexible, with variations in the inter-Cα distance on the

order of 10 Å, the two ends form a salt bridge and stay within 3.4 Å of each other for 83% of the simulation. Despite the apparent large-scale motion of the intervening remnant of ICL3, the root mean-square fluctuation (RMSF) of TM5 and TM6 is <2 Å. The RMSF is a measure of the fluctuations for each atom about the mean structure, averaged over time; this is distinct from the RMSD, which is the average deviation over all atoms at a specific time point. As shown in Fig. S1 in the Supporting Material, the centers of the helices are remarkably rigid, with an RMSF of ~0.5 Å. Moreover, a comparison of the RMSF for comparable TM Cα atoms between a dark-state rhodopsin simulation and the current B2AR simulation shows that not only are the central residues of TM5 and TM6 more mobile in rhodopsin than B2AR, but the end of TM5 in rhodopsin has an up to 2 Å greater RMSF than B2AR (28).

A principal-components analysis (PCA) of the trajectory yields a set of vectors (principal components (PCs)) that give the direction of motion about the average conformation, as well as information about correlations between motions. This is easily visualized as a “porcupine” plot in which the individual atom vectors are mapped onto the average structure. Although the relative sizes of the vectors are indicative of the relative magnitude of the fluctuations from the average position for each mapped atom, the vectors have been scaled by a factor of 25 for easy visualization. It is therefore important to keep in mind that, in the context of this discussion, we refer to “large-scale” as a synonym for “concerted”, meaning that a large number of atoms are moving in concert. The magnitudes of the motions described here are relatively small, as indicated by the above discussion about RMSD and RMSF.

Fig. 1 shows porcupine plots for B2AR in which the first PC, corresponding to the largest concerted motions of the TM Cα atoms, has been mapped onto the average structure. The left panel shows B2AR from the EC side. There is concerted motion at the EC end of TM6 toward the core of the protein that is consistent with earlier MD studies by Huber et al. (30) in which a bound carazolol was exchanged

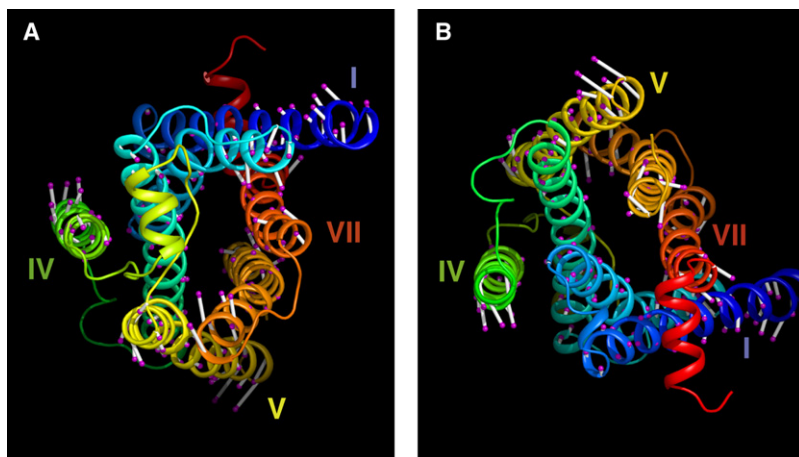


FIGURE 1 First principal component This figure shows a “porcupine plot” based on the PCA of the TM Cαs from the simulation. The first PC is shown here as “matchsticks” projecting from the average structure. Panel A shows a view from the EC side, and panel B shows a view from the IC side. Projecting the ensemble onto these vectors shows that the trend is movement from the base of the matchstick to the tip.

with epinephrine. There is also an inward tilting of the EC end of TM3. In fact, TM1 and TM3, and TM5 and TM6 appear to “rock” past each other on the EC side. The right panel of Fig. 1 shows the view of B2AR from the IC side. Of particular note here is the movement of the IC end of TM5 away from TM6, the apparent rotation of TM6 (described in more detail in the “Ionic lock” section below), and the movement of TM7 away from the core of the protein.

These motions, and in particular the movements of TM6 and TM7, seem consistent with those observed experimentally to be associated with activation in GPCRs. We see what could be construed as a “tilting” inward of the EC ends of TM6 and TM3 along with a rotation of the IC end of TM6 that looks remarkably like the motion of TM6 proposed by Farrens and co-workers (31) for light activation of rhodopsin. Although a later study suggested that this movement is more likely a rectilinear motion of TM6 away from the center of the protein due to steric clashes in the tilt and rotation model, the tilt and rotation model is not otherwise inconsistent with the experimental data (32). Furthermore, electron paramagnetic resonance experiments suggest that during rhodopsin activation, the cytoplasmic end of TM7 moves relative to the cytoplasmic end of TM1 (with little change in the TM1-to-H8 distances) (32,33). Although the motion we see in TM7 is not directly away from TM1, there does appear to be a relative movement of the two ends apart from each other, with the movement coming largely from a shift in TM7.

The RMSD map is a graphical representation of the conformational variability of the system (in this case, the TM C $\alpha$ s) as well as the presence of conformational substates. These substates appear as dark blocks along the diagonal, where the structures within a block are all similar to each other. Off-diagonal blocks indicate that the system revisits similar conformations, and large off-diagonal blocks imply that a conformational substate has been revisited. This block structure is a qualitative clustering method and reflects the underlying energy surface for the molecule (34–36).

The RMSD map for the TM helices of B2AR is shown in Fig. 2 A. The mean RMSD from the map was 1.1 Å with a maximum of 1.9 Å, indicating that the protein core is

extremely rigid—it is readily apparent that the TM helices of B2AR simply do not move very much. Despite this lack of motion, there is a well-defined diagonal block structure to the RMSD map, showing ~4 clusters at ~0–180 ns, 200–650 ns, 660–825 ns, and 830–1023 ns. The largest of these blocks lasted for ~400 ns. In addition, there are some cross-peaks between the second and fourth clusters, indicating that these substates are quite similar.

For comparison purposes, the equivalent RMSD map for the dark-state rhodopsin is shown in Fig. 2 B; it has an average RMSD of 1.6 Å and a maximum of 3.2 Å (28). The rhodopsin RMSD map also shows a block-diagonal structure, though less distinctly than B2AR. More striking is the degree of motion in comparison to B2AR. Although one might be tempted to conclude that the rhodopsin structure is drifting, the RMSD between the simulation and the starting crystal structure shows only a slight drift of 0.5 Å over the first 400 ns, and then is level for the remaining 1.2  $\mu$ s. Based on these data and a PCA of the global conformational substates (see the Supporting Material), we conclude that the simulation of B2AR is nonergodic even after 1  $\mu$ s, that is, its accessible conformational space has not yet been fully sampled (37–39). This serves as a reminder of the innate challenge of getting good statistics from MD simulations of macromolecules (38,39).

That rhodopsin exhibited significantly larger fluctuations came as a major surprise. The classical view of B2AR is that it exists in a set of conformational substates, with some degree of flexibility permitting interconversion between substates as well as ligand ingress, given that B2AR can spontaneously activate (2,5). In contrast, rhodopsin requires a very high signal/noise ratio for its function as a photon sensor, and as such is stably locked, with no spontaneous activation in the absence of light. One would therefore expect the dark-state rhodopsin simulation to have a lower RMSD than B2AR, yet this is not the case. It is possible that differences in the membrane composition between the rhodopsin and B2AR simulations could manifest as a decrease in TM RMSD. However, this seems unlikely, as the helical motions indicated in the PCA (tilts, rotations, and rigid-body shifts) are inconsistent with what one would expect if the membrane were to exert

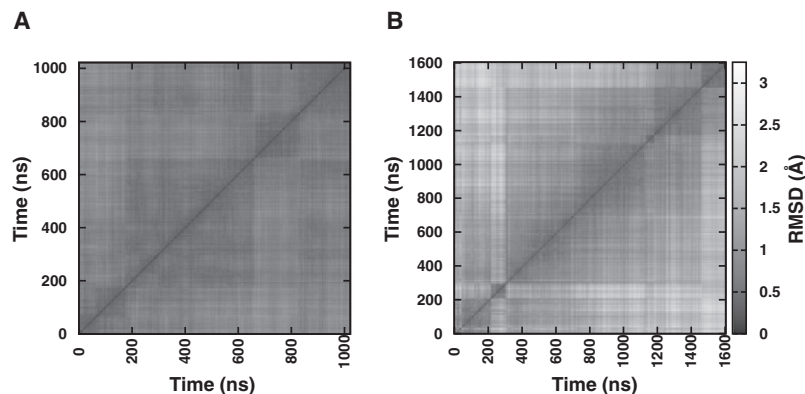


FIGURE 2 TM C $\alpha$  RMSD maps. This figure shows the RMSD maps for TM C $\alpha$ s from B2AR (A) and dark rhodopsin (B). The diagonal-block structure is indicative of the protein exploring local substates (i.e., ensembles of similar conformations). The scaling is identical between the panels, showing that the conformational variation in B2AR is 30% smaller on average, and 40% smaller based on the peak RMSD.

an increase in lateral pressure. It has been pointed out that the short helical stretch in the second EC loop (ECL2) of B2AR, along with its two disulfide bonds, may stabilize the core of the protein (6). Rhodopsin lacks this helical element in its ECL2 and only has one disulfide bond linking it with TM3. It is possible that these structural differences also contribute to the smaller-magnitude motions seen in B2AR.

### Water distribution and average structure

There is evidence that water plays an important role in the structure and function of GPCRs (28,40–42). Internal waters have been found in the crystal structures of B2AR, B1AR, and A2A (6,12,13). Moreover, previous simulations of rhodopsin have shown that its core is highly hydrated, and that the amount of water within the core of the protein changes with activation (28). In addition, short-timescale simulations of a predicted apo-B2AR structure, solvated and in a membrane, have also shown the presence of a solvent channel (43). To better understand the spatiotemporal distribution of waters in the simulation, we constructed a “density map”, which is essentially a 3D histogram of waters that shows where they have been over the course of a simulation. To restrict the visualization to waters that are likely to be internal to the core of the protein, we only considered waters that were within 15 Å of the protein’s principal axis, computed from only the  $\alpha$ -carbon positions of the TM helices.

The water density distribution for B2AR is shown in Fig. 3 A, along with a comparison between the crystallographic structure (in *blue*) and the simulation average structure (in *yellow*). The carazolol ligand from the crystal structure is shown in green and the crystallographic waters are depicted as red spheres. To eliminate the bulk solvent at the ends of the protein core, a clipping plane in the *z*-dimension was used to exclude bulk waters. It is important to note that this representation does not distinguish between a single water occupying

a site for the duration of the simulation and a site in which water constantly exchanges frequently; only the overall rate of occupancy matters. With this scheme, the bulk water density level was  $\approx 0.7$  and the water density maps were therefore contoured at half-bulk, or 0.35.

We find that the core of the protein is significantly hydrated, including the pocket where carazolol is bound. There are  $97 \pm 7$  waters, on average, within the core of the protein. In addition, the density values for the water found in the carazolol pocket are higher than they are virtually anywhere else within the protein core. A number of the waters within the core have quite long lifetimes—one water was continuously internal for 639 ns, and 17 others spent  $>100$  ns inside. In addition, the water surface near the middle of the core lies near the highly conserved NPxxY motif of TM7 (41,44). Of the six crystallographic waters in this region, four are contained within the simulation water density surface, and two are within  $\sim 2$  Å of the surface. This region also shows a higher average water density (i.e., higher water occupancy) than is seen elsewhere within the core.

A comparison of the simulation average with the crystal structure shows a shift of the average TM7 that is quite pronounced at the cytoplasmic end, where the void left by the end of TM7 is filled with water. When the clipping plane is removed, this region of water is found to be part of a projection up from the bulk solvent through the center of the cytoplasmic end of the protein and then out between the cytoplasmic ends of TM6 and TM7. The density then fuses with a “finger” of water density reaching up from the bulk solvent but along the exterior of the protein. Plots with lower contour values for the solvent density show that these two paths are in fact channels that connect from the cytoplasmic side bulk density up through the structural water region around the NPxxY motif, through the carazolol-binding region, and into the EC side bulk water density. It is possible that the charged internal residues do contribute

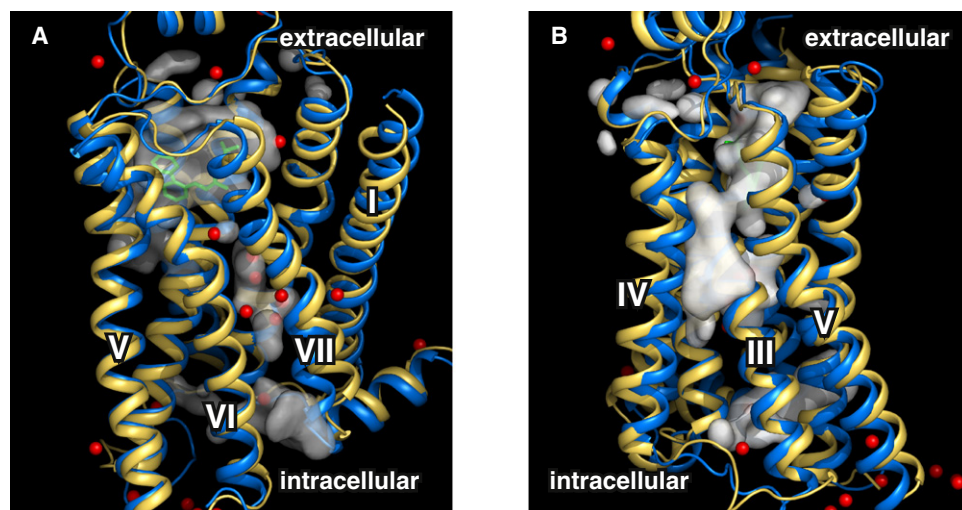


FIGURE 3 Comparison between the x-ray crystal structure (*blue*) and the simulation average (*yellow*). The carazolol ligand (present in the x-ray structure but not in the simulation) is shown in green. The crystallographic waters are shown as red spheres. The protein core water density from the simulation, contoured at half of bulk density, is shown as the translucent surface. Panel A shows a view from in front of TM6 with the NPxxY motif near the TM7 label. Panel B shows the back of the structure (rotated 180° about the vertical axis). To clarify viewing, the water density was made more opaque in B.

some to the hydration that we see. However, a similar hydration pattern, including a water channel entering from the cytoplasmic side around the conserved D(E)RY and NPxxY motifs, was seen in previous simulations of rhodopsin (28). Fig. 3 B shows the protein rotated  $\approx 180^\circ$  about the membrane normal. In this case, the solvent density surface has been made slightly more opaque to aid in visualization. There is a pronounced translation of the average TM4 conformation away from TM5 and TM3, relative to the crystal structure, with the intervening space again filled with a large “finger” of water density.

### Ionic lock

In contrast to the crystal structures of GPCRs, long-timescale MD simulations of B2AR show the ionic lock reforming (45,46). Dror et al. (45) found that the lock rapidly reformed, but the association varied from a slightly noisy lock to significant transitions between the opened and closed states depending upon the simulation. In our simulation, we found that the lock very rapidly reformed during the equilibration phase and stayed in a noisy, restricted state until  $\sim 650$  ns into the simulation. At this point, the lock broke and then reformed  $\sim 200$  ns later. This is described in the bottom panel of Fig. 4, which shows the distance between the amine (NH1) of R131 and the carboxyl oxygens (OE1 and OE2) of E268 over the course of the simulation. The opening and closing of the lock is not entirely surprising, given that apo-B2AR exhibits a moderate level of basal activity, and the partial inverse agonist carazolol has been removed.

For comparison, the distance between the corresponding residues (R135 and E247) in a simulation of dark-state rhodopsin is shown in the middle panel of Fig. 4 (28). Here, the

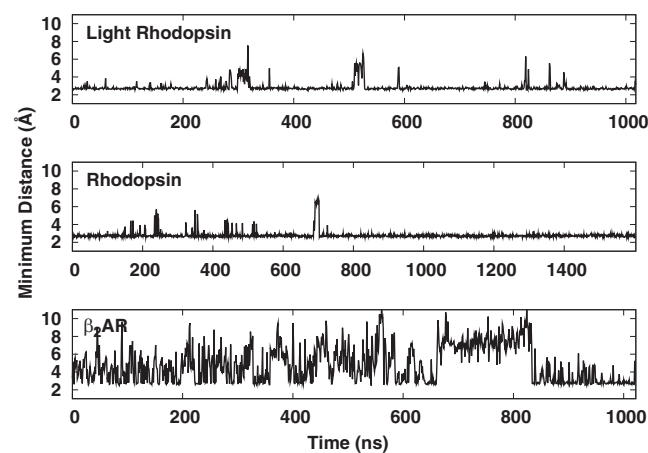


FIGURE 4 Ionic lock from B2AR and rhodopsin. The minimum distances between any atom in the residues that comprise the “ionic lock” for B2AR and rhodopsin are plotted here. The bottom panel shows the state of the ionic lock (R131–E268) for B2AR over the course of the simulation. The middle panel shows the ionic lock for a dark rhodopsin simulation (R135–E247), and the bottom panel shows the ionic lock from the light rhodopsin simulation.

lock remains very stably closed, as expected, because to function effectively as a dim-light receptor, rhodopsin needs to be kept inactive when there are no photons present to maintain a high signal/noise ratio. The top panel shows the lock from a rhodopsin simulation after isomerization of the retinal, with a corresponding increase in “noise” in the lock (28).

The probability distribution of the ionic lock distance can be broken down into three states: “locked”, semiopen with a single bridging water, and fully open. A distance of  $< 3.2$  Å is considered to be “locked”. One can then classify distances  $\geq 3.2$  Å as having a bridging water or not by using a distance search for any water that is within hydrogen-bonding distance of both sides of the lock. The distribution of these states is depicted in Fig. 5. The “bridging-water” lock states coincide with the first “bump” in the distribution covering lock distances from 3.2 Å to 5.5 Å.

The water-bridged state is a very short-lived state with a lifetime of  $< 1$  ns. The time series for the locked states is shown in Fig. S6. Considering only the typical salt-bridge distance of 3.2 Å as a classification would suggest that the lock is frequently open, as in Fig. 4. In contrast, Fig. S6 shows that the lock rapidly interconverts among all three states during the first half of the simulation, and that during a sizable fraction of the time it would normally be considered open, it is in fact associating with a water between the two sides of the lock. This association imposes a conformational restriction on the lock, and therefore, even though the lock is not closed, it is not as free as a fully open lock would be.

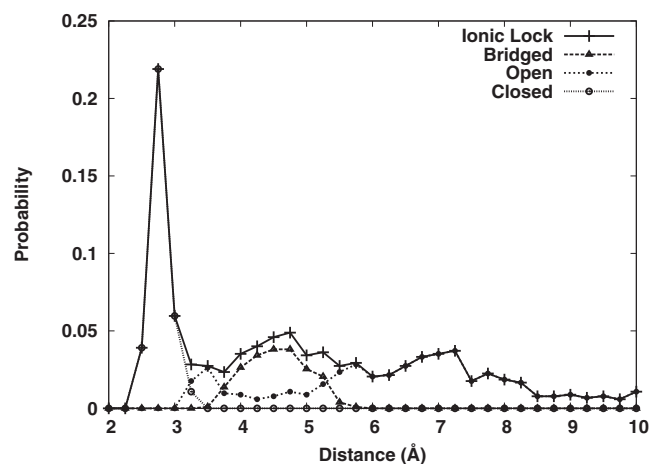


FIGURE 5 Ionic lock and bridging water. This figure shows the distribution of the distances between the two residues of the ionic lock (solid line), measured by the distance between the E268 side-chain oxygens and the nitrogen of R131. The ionic lock is then classified as having a bridging water (hydrogen bonding to both sides of the lock), whose distribution is shown by the dashed line, or no bridging water. Ionic lock conformations that lack a bridging water and are  $> 3.2$  Å apart are depicted by the dotted line. The thin dotted line shows states that are closed (i.e.,  $< 3.2$  Å apart). This shows that the ionic lock exists in three states: “locked”, open but with a bridging water, and fully open.

In the case of B2AR, the lock-breaking event is followed by a reorganization of the cytoplasmic end of TM6, whereupon the lock reforms. This event is not simply a local fluctuation or a change in the orientation of the side chains of the lock constituents, as demonstrated by the top two panels of Fig. 6. The top panel shows the projection of TM6's motion along its first PC computed only from the C $\alpha$ s. The middle panel shows the lock distance. It is clear that the lock opening corresponds to a concerted motion of the TM6 C $\alpha$  trace, as evidenced by the PCA mode. Considering that the cytoplasmic end of TM6 is connected to ICL3, which was absent in our simulation, it is of some concern that this event and reorganization could be an artifact of this change in the structure, particularly since the ends of the linkers to ICL3 were left broken. The bottom panel of Fig. 6 shows the distance between the C $\alpha$ s at either end of the clip. There is a large motion of the termini apart from each other at 450 ns. However, by 600 ns, they have reassociated, and it is not until 50 ns later that the lock breaks. There is also no significant movement of the TM6 C $\alpha$ s, as evidenced by the PC plot, before the lock-breaking event.

The reorganization of the cytoplasmic end of TM6 is reflected in the global conformational substates as defined by the PCA. Fig. S2 shows the phase space portrait defined by the three most significant PCs. It is clear that the lock opening in fact corresponds to a distinct global substate, as shown by the magenta "bead". This suggests that what we are seeing is an activation-precursor event corresponding to a breaking of the lock and a reorganization of the cytoplasmic end of TM6, coupled with a larger-scale reorganization within the TM helices. Indeed, many studies have shown that agonists induce a movement in the cytoplasmic end of TM6 (2,31,32,47).

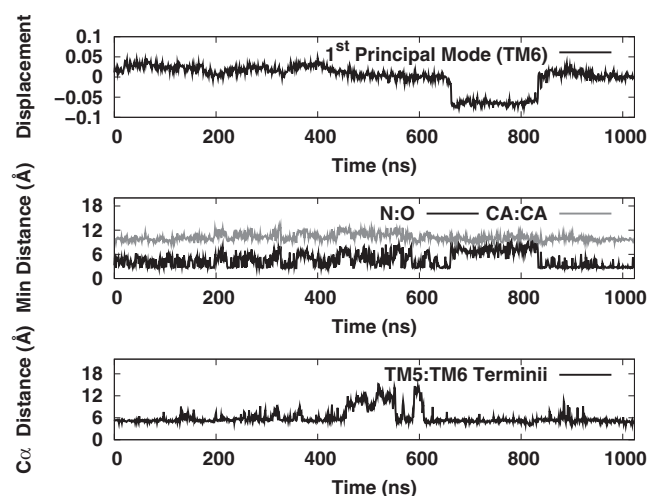


FIGURE 6 Ionic lock detail in B2AR. The top panel shows a projection of TM6 along its first PC. The middle panel shows the N-O and C $\alpha$ -C $\alpha$  distance between R131 and E268 in B2AR. The bottom panel shows the distance between the C $\alpha$  at the termini of TM5 and TM6 where the ICL3 was clipped.

Finally, the RMSD along the first PC (see Fig. S5) shows a large displacement that corresponds to the lock-opening region, but no movement during the ICL3 reorganization. The second mode, however, shows a large displacement during the ICL3 reorganization. This further suggests that global conformational changes associated with the ICL3 reorganization are independent of those associated with the lock opening. We are therefore confident that the movement of the termini and the lock breaking are independent events.

Of interest, the C $\alpha$ -C $\alpha$  distance between E268 and R131, shown in Fig. 6, does not seem to indicate a change in the backbone about the lock in TM6. Closer examination, however, reveals that there is in fact a clockwise rotation of the entire IC end of TM6, as seen from the cytoplasm. This is shown in Fig. 7. The left panel (A) shows the lock just before opening at 645 ns into the simulation. The right panel (B) shows the lock just after opening at 677 ns. Here, the clockwise rotation of the helix is readily apparent. The IC end essentially unwinds to form a small section of  $\pi$ -helix and then rewinds when the lock closes.

It is important to note that the PCs shown in Fig. 1 characterize the global motion of the protein over the course of the simulation, and as such encompass the global motions associated with lock opening as well as lock closing. It is possible to elucidate the global motions related to the lock transition event by computing the PCA on either side of the event, i.e., 550 ns to 750 ns to capture the opening of the lock and 750 ns to 950 ns to capture the closure of the lock. This is shown in Fig. 8, where we find that the EC ends of TM3 and TM6 move inward toward each other in the direction of ECL2. There is also an indication of movement of the extreme EC end of TM7 moving inward toward the center of the protein, and hence toward the convergence point of TM3 and TM6. This motion appears consistent with metal ion binding studies that showed movement of the EC ends of TM3, TM6, and TM7 as part of activation (48). In addition, the unwinding and winding of the IC end of TM6 is shown to correlate with the lock opening and closing, as well as with a concomitant movement of the IC end of TM5 away from TM6. Perhaps what is most striking about these motions is that the PCs for the lock closing point in almost exactly the opposite direction as those for the lock opening. The EC ends of TM3 and TM6 move apart, as does the EC end of TM7, though again with less coherence than the other two helices.

There is evidence that the intrahelical salt bridge of the (D/E)RY motif is more important for stabilizing the inactive conformation of rhodopsin than the interhelical salt bridge between TM3 and TM6 (11). In our simulation, the D130-R131 salt bridge exists through the entire trajectory with an average distance of 2.8 Å. Periodically, the D130 moves as far as 6 Å away from R131, but this generally lasts for <2 ns, after which the salt bridge is reformed. Although the frequency of these disruptions increases slightly over

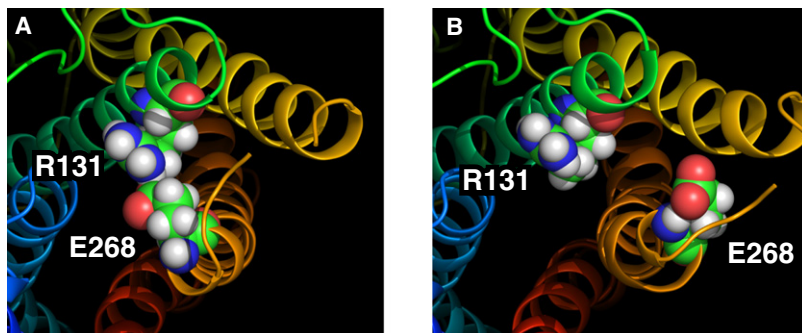


FIGURE 7 Ionic lock in B2AR. This figure shows the conformation of the ionic lock in B2AR from the IC side. Panel *A* shows the lock at 645 ns into the simulation with the lock closed. Panel *B* shows the lock at 677 ns with the lock open. A clockwise rotation of the IC end of TM6 is clearly visible accompanying the lock opening.

time, there is no apparent correlation between them and the interhelical lock breaking and reforming.

## CONCLUSIONS

We have used a 1.02  $\mu$ s MD simulation of an apo-B2AR protein with a clipped ICL3 to characterize the fluctuations

and conformations accessible to the protein—in particular, the TM helices and the ionic lock. We have shown that, in contrast to the extant crystal structures, the lock rapidly reforms. Moreover, the lock breaks and reforms along with concomitant conformational changes within the TM helices that are consistent with existing biochemical evidence and hypothesized models for conformational changes associated

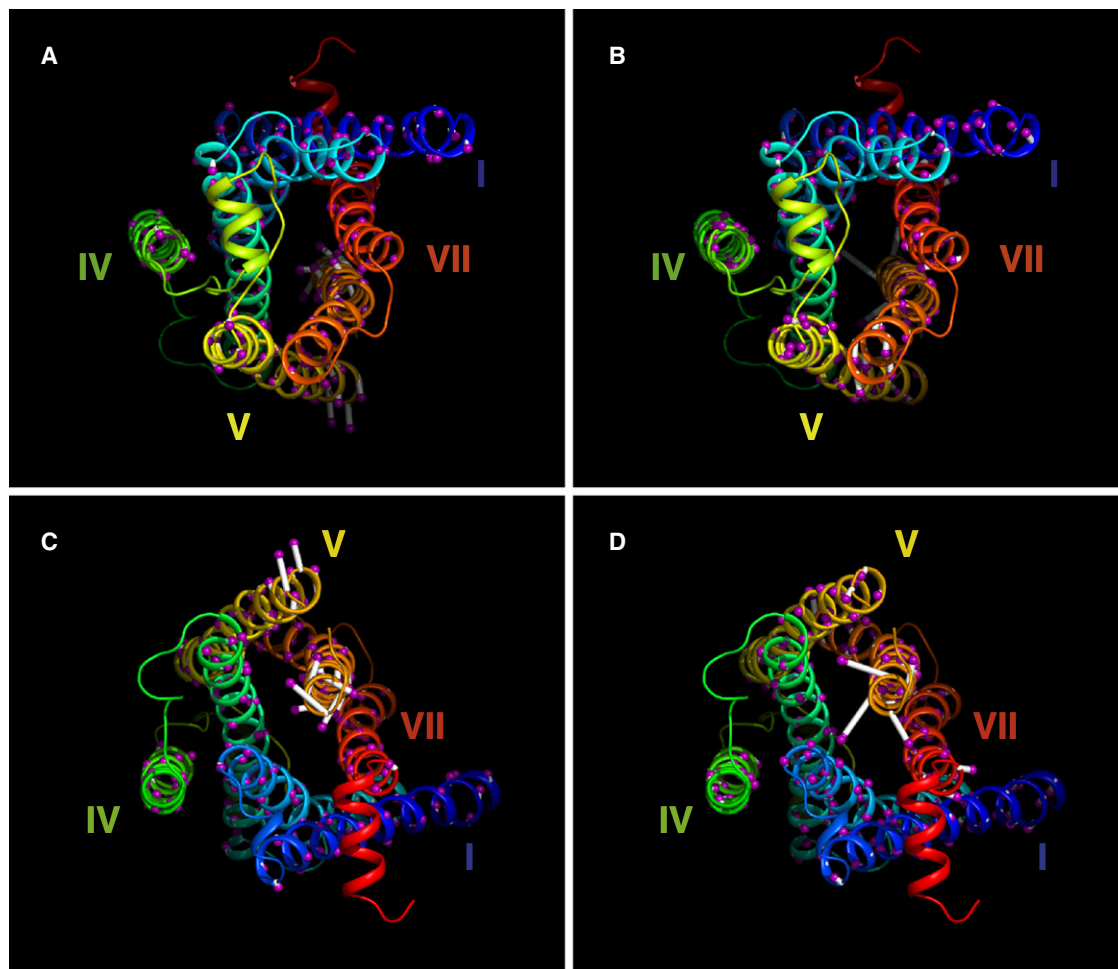


FIGURE 8 PCA of ionic lock opening and closing. This figure shows a “porcupine” plot based on the PCA of the TM C $\alpha$ s from 550 ns to 750 ns, corresponding to the lock opening, and from 750 ns to 950 ns, corresponding to the lock closing. Panel *A* shows a view of the lock opening from the EC side, and panel *B* shows the lock closing from the same side. Panel *C* shows the lock opening viewed from the cytoplasmic side, and panel *D* shows the lock closing from the same view. The eigenvectors are scaled here by a factor of 15 to enhance visibility.

with activation. The EC ends of TM3, TM6, and TM7 move inward toward each other while the IC end of TM5 moves away from TM6. In addition, the IC end of TM6 unwinds slightly with a clockwise rotation, opening the lock. We found the magnitude of the fluctuations of B2AR to be surprisingly small—many of the “activation-precursor” motions associated with the ionic lock breaking are, in fact, quite subtle. Finally, we find that the ionic lock can be described by three states: closed (or locked), semi-open with a bridging water, and fully open.

The interior of B2AR, including the vacant carazolol location and the region around the conserved NPxxY motif in TM7, is well hydrated. In fact, our simulations indicate that the locations within the B2AR core with the highest water occupancies agree well with the crystallographically determined waters. Many of the structural differences seen between the average simulation structure and the x-ray crystallographic structure, such as the moving apart of TM4 and TM5, could be attributed to this hydration. This extensive hydration provides ample space for side-chain reorganization that would accompany binding and activation, and may better reflect the operational environment of the protein at physiologic temperatures than the degree of hydration found in the crystal would suggest.

Our results show agreement among the simulation and crystallographic data and biochemical experiments. The characterization of motions associated with the toggling of the ionic lock may provide a better understanding of the structural changes involved in activation of B2AR.

## SUPPORTING MATERIAL

Methods and results, references, and six figures are available at [http://www.biophysj.org/biophysj/supplemental/S0006-3495\(09\)01558-6](http://www.biophysj.org/biophysj/supplemental/S0006-3495(09)01558-6).

We thank Arnau Cordero and Brian Kobilka for insightful discussions, and Xavier Deupi for discussions and a critical reading of this manuscript. We also thank the IBM Watson Research Center and the Computational Biology Center for use of the BGW BlueGene supercomputer. We extend a special thanks to the Blue Matter development team (B. Fitch, R. Germain, A. Rayshubskiy, T. J. C. Ward, M. Eleftheriou, F. Suits, Y. Zhestkov, R. Zhou, J. Pitera, and W. Swope). We would also like to thank Warren Delano for PyMOL, which was used in preparing some of the figures in this article.

## REFERENCES

- Kobilka, B. K. 2007. G protein coupled receptor structure and activation. *Biochim. Biophys. Acta.* 1768:794–807.
- Kobilka, B. K., and X. Deupi. 2007. Conformational complexity of G-protein-coupled receptors. *Trends Pharmacol. Sci.* 28:397–406.
- Lefkowitz, R. J. 2000. The superfamily of heptahelical receptors. *Nat. Cell Biol.* 2:E133–E136.
- Fredriksson, R., and H. B. Schiöth. 2005. The repertoire of G-protein-coupled receptors in fully sequenced genomes. *Mol. Pharmacol.* 67: 1414–1425.
- Rosenbaum, D. M., S. G. Rasmussen, and B. K. Kobilka. 2009. The structure and function of G-protein-coupled receptors. *Nature.* 459: 356–363.
- Cherezov, V., D. M. Rosenbaum, ..., R. C. Stevens. 2007. High-resolution crystal structure of an engineered human  $\beta$ 2-adrenergic G protein-coupled receptor. *Science.* 318:1258–1265.
- Rasmussen, S. G., H. J. Choi, ..., B. K. Kobilka. 2007. Crystal structure of the human  $\beta$ 2 adrenergic G-protein-coupled receptor. *Nature.* 450:383–387.
- Rosenbaum, D. M., V. Cherezov, ..., B. K. Kobilka. 2007. GPCR engineering yields high-resolution structural insights into  $\beta$ 2-adrenergic receptor function. *Science.* 318:1266–1273.
- Ballesteros, J. A., A. D. Jensen, ..., J. A. Javitch. 2001. Activation of the  $\beta$ 2-adrenergic receptor involves disruption of an ionic lock between the cytoplasmic ends of transmembrane segments 3 and 6. *J. Biol. Chem.* 276:29171–29177.
- Palczewski, K., T. Kumasaka, ..., M. Miyano. 2000. Crystal structure of rhodopsin: a G protein-coupled receptor. *Science.* 289:739–745.
- Vogel, R., M. Mahalingam, ..., T. P. Sakmar. 2008. Functional role of the “ionic lock”—an interhelical hydrogen-bond network in family A heptahelical receptors. *J. Mol. Biol.* 380:648–655.
- Warne, T., M. J. Serrano-Vega, ..., G. F. Schertler. 2008. Structure of a  $\beta$ 1-adrenergic G-protein-coupled receptor. *Nature.* 454:486–491.
- Jaakola, V. P., M. T. Griffith, ..., R. C. Stevens. 2008. The 2.6 angstrom crystal structure of a human A2A adenosine receptor bound to an antagonist. *Science.* 322:1211–1217.
- Park, J. H., P. Scheerer, ..., O. P. Ernst. 2008. Crystal structure of the ligand-free G-protein-coupled receptor opsin. *Nature.* 454:183–187.
- Hanson, M. A., and R. C. Stevens. 2009. Discovery of new GPCR biology: one receptor structure at a time. *Structure.* 17:8–14.
- Rubenstein, R. C., S. K. F. Wong, and E. M. Ross. 1987. The hydrophobic tryptic core of the  $\beta$ -adrenergic receptor retains Gs regulatory activity in response to agonists and thiols. *J. Biol. Chem.* 262:16655–16662.
- Brooks, B. R., R. E. Bruccoleri, ..., M. Karplus. 1983. CHARMM: a program for macromolecular energy, minimization, and dynamics calculations. *J. Comput. Chem.* 4:187–217.
- MacKerel, Jr., A. D., D. Bashford, ..., M. Karplus. 1998. All-atom empirical potential for molecular modeling and dynamics studies of protein. *J. Phys. Chem. B.* 102:3586–3616.
- Feller, S. E., K. Gawrisch, and A. D. MacKerell, Jr. 2002. Polyunsaturated fatty acids in lipid bilayers: intrinsic and environmental contributions to their unique physical properties. *J. Am. Chem. Soc.* 124:318–326.
- Klauda, J. B., B. R. Brooks, ..., R. W. Pastor. 2005. An ab initio study on the torsional surface of alkanes and its effect on molecular simulations of alkanes and a DPPC bilayer. *J. Phys. Chem. B.* 109:5300–5311.
- Deserno, M., and C. Holm. 1998. How to mesh up Ewald sums. II. An accurate error estimate for the particle-particle-particle-mesh algorithm. *J. Chem. Phys.* 109:7694–7701.
- Deserno, M., and C. Holm. 1998. How to mesh up Ewald sums. I. A theoretical and numerical comparison of various particle mesh routines. *J. Chem. Phys.* 109:7678–7693.
- Andersen, H. C. 1983. RATTLE: a “velocity” version of the SHAKE algorithm for molecular dynamics calculations. *J. Comput. Chem.* 52:24–34.
- Phillips, J. C., R. Braun, ..., K. Schulten. 2005. Scalable molecular dynamics with NAMD. *J. Comput. Chem.* 26:1781–1802.
- Fitch, B. G., R. S. Germain, ..., R. Zhou. 2003. Blue Matter, an application framework for molecular simulation on Blue Gene. *J. Para. Distrib. Comp.* 63:759–773.
- Allen, F., G. Almasi, ..., R. Zhou. 2001. Blue Gene: a vision for protein science using a petaflop supercomputer. *IBM Syst. J.* 40:310–327.
- Grossfield, A., S. E. Feller, and M. C. Pitman. 2006. A role for direct interactions in the modulation of rhodopsin by  $\omega$ -3 polyunsaturated lipids. *Proc. Natl. Acad. Sci. USA.* 103:4888–4893.
- Grossfield, A., M. C. Pitman, ..., K. Gawrisch. 2008. Internal hydration increases during activation of the G-protein-coupled receptor rhodopsin. *J. Mol. Biol.* 381:478–486.

29. Romo, T.D., and A. Grossfield. 2009. LOOS: an extensible platform for the structural analysis of simulations. *Proc. Int. IEEE EMBS Conf., 31st.* 2232–2335.
30. Huber, T., S. Menon, and T. P. Sakmar. 2008. Structural basis for ligand binding and specificity in adrenergic receptors: implications for GPCR-targeted drug discovery. *Biochemistry.* 47:11013–11023.
31. Farrens, D. L., C. Altenbach, ..., H. G. Khorana. 1996. Requirement of rigid-body motion of transmembrane helices for light activation of rhodopsin. *Science.* 274:768–770.
32. Altenbach, C., A. K. Kusnetzow, ..., W. L. Hubbell. 2008. High-resolution distance mapping in rhodopsin reveals the pattern of helix movement due to activation. *Proc. Natl. Acad. Sci. USA.* 105:7439–7444.
33. Altenbach, C., K. Cai, ..., W. L. Hubbell. 2001. Structure and function in rhodopsin: mapping light-dependent changes in distance between residue 65 in helix TM1 and residues in the sequence 306–319 at the cytoplasmic end of helix TM7 and in helix H8. *Biochemistry.* 40:15483–15492.
34. García, A. E. 1992. Large-amplitude nonlinear motions in proteins. *Phys. Rev. Lett.* 68:2696–2699.
35. Hess, B. 2000. Similarities between principal components of protein dynamics and random diffusion. *Phys. Rev. E.* 62(6 Pt B):8438–8448.
36. Hess, B. 2002. Convergence of sampling in protein simulations. *Phys. Rev. E.* 65:031910.
37. Clarage, J. B., T. Romo, ..., G. N. Phillips, Jr. 1995. A sampling problem in molecular dynamics simulations of macromolecules. *Proc. Natl. Acad. Sci. USA.* 92:3288–3292.
38. Grossfield, A., S. E. Feller, and M. C. Pitman. 2007. Convergence of molecular dynamics simulations of membrane proteins. *Proteins.* 67:31–40.
39. Grossfield, A., and D. M. Zuckerman. 2009. Quantifying uncertainty and sampling quality in biomolecular simulations. *Ann. Rep. Comput. Chem.* 5:23–48.
40. Okada, T., Y. Fujiyoshi, ..., Y. Shichida. 2002. Functional role of internal water molecules in rhodopsin revealed by X-ray crystallography. *Proc. Natl. Acad. Sci. USA.* 99:5982–5987.
41. Pardo, L., X. Deupi, ..., M. Campillo. 2007. The role of internal water molecules in the structure and function of the rhodopsin family of G protein-coupled receptors. *ChemBioChem.* 8:19–24.
42. Jardón-Valadez, E., A. N. Bondar, and D. J. Tobias. 2009. Dynamics of the internal water molecules in squid rhodopsin. *Biophys. J.* 96:2572–2576.
43. Spijker, P., N. Vaidehi, ..., W. A. Goddard, 3rd. 2006. Dynamic behavior of fully solvated  $\beta$ 2-adrenergic receptor, embedded in the membrane with bound agonist or antagonist. *Proc. Natl. Acad. Sci. USA.* 103:4882–4887.
44. Mirzadegan, T., G. Benkő, ..., K. Palczewski. 2003. Sequence analyses of G-protein-coupled receptors: similarities to rhodopsin. *Biochemistry.* 42:2759–2767.
45. Dror, R. O., D. H. Arlow, ..., D. E. Shaw. 2009. Identification of two distinct inactive conformations of the  $\beta$ 2-adrenergic receptor reconciles structural and biochemical observations. *Proc. Natl. Acad. Sci. USA.* 106:4689–4694.
46. Vanni, S., M. Neri, ..., U. Rothlisberger. 2009. Observation of “ionic lock” formation in molecular dynamics simulations of wild-type  $\beta$ 1 and  $\beta$ 2 adrenergic receptors. *Biochemistry.* 48:4789–4797.
47. Altenbach, C., J. Klein-Seetharaman, ..., W. L. Hubbell. 2001. Structure and function in rhodopsin: mapping light-dependent changes in distance between residue 316 in helix 8 and residues in the sequence 60–75, covering the cytoplasmic end of helices TM1 and TM2 and their connection loop CL1. *Biochemistry.* 40:15493–15500.
48. Schwartz, T. W., T. M. Frimurer, ..., C. E. Elling. 2006. Molecular mechanism of 7TM receptor activation—a global toggle switch model. *Annu. Rev. Pharmacol. Toxicol.* 46:481–519.